SCIENCE CHINA
Chemistry

• ARTICLES •

June 2016 Vol.59 No.6: 740–745
doi: 10.1007/s11426-015-5550-3

Uranyl oxamate hydrates: hydrothermal synthesis, crystal structure, photophysical properties, and selective crystallization

Yubo Shu[1,2] & Weisheng Liu[1*]

[1]*College of Chemistry and Chemical Engineering, Lanzhou University, Lanzhou 730000, China*
[2]*School of Chemical and Biological Engineering, Hechi University, Yizhou 546300, China*

Received July 16, 2015; accepted August 28, 2015; published online May 12, 2016

Presented here are two isostructural uranyl coordination polymers $[UO_2(EDO)(H_2O)]\cdot H_2O$ (**1**) and $[UO_2(BDO)(H_2O)]\cdot 2H_2O$ (**2**) (EDO^{2-}=ethylene-1,2-dioxamate; BDO^{2-}=butylene-1,2-dioxamate) with identical stepwise zigzag chain structure and distinct interchain hydrogen bonding interaction, prepared from hydrothermal reaction of DEEDO or DEBDO (DEEDO= diethyl ethylene-1,2-dioxamate; DEBDO=diethyl butylene-1,2-dioxamate) with uranyl ions. The monomeric uranyl-based fluorescence emissions of compounds **1** and **2** are red-shifted by about 6 and 5 nm respectively, compared to that of uranyl nitrate hexahydrate. Compound **1** has stronger emission than compound **2**, but both their emissions exhibit triple-exponential decay. The photophysics of uranyl oxalate trihydrate was also investigated for comparison. The selective crystallization of compound **1** in alkaline solution was applied to the sequestration of uranyl ions, showing a kinetic preference.

uranium, oxamate, hydrothermal synthesis, photophysics, selective crystallization

Citation: Shu YB, Liu WS. Uranyl oxamate hydrates: hydrothermal synthesis, crystal structure, photophysical properties, and selective crystallization. *Sci China Chem*, 2016, 59: 740−745, doi: 10.1007/s11426-015-5550-3

1 Introduction

With the development of supramolecular chemistry and crystal engineering, there has been a resurgent interest for uranyl-organic complexes because of their unique building units and interesting photoactive properties [1–4], as well as the observation of the interaction between uranium(VI) and organic species, which is related to uranyl extraction in soil decontamination and nuclear-waste reprocessing [5–7]. Recently, more efforts have been devoted to exploiting the incorporation of supramolecular interactions (such as hydrogen and halogen bonding) into the design and assembly of uranyl complexes, because these weak interactions not only influence on the structural topologies and dimensionality [2], but also play subtle effects on the bulk properties [8,9].

Uranyl luminescence, originating from ligand-to-metal charge transfer (LMCT) transition involving promotion of an electron from the highest occupied molecular orbital (HOMO) 6d-5f-2p U–O $3\sigma_u$ bond to the lowest unoccupied molecular orbital (LUMO) nonbonding uranium(VI) $5f_\delta$ and $5f_\phi$ orbitals [10], is of great theoretical significance because it possesses both actinide f-characterized long excited state lifetime and ligand L-characterized variable HOMO-LUMO energy gap. However, until now, theoretical studies of uranyl photophysics have been mainly limited to the free uranyl ion. As for more complicated photophysical process in uranyl complexes, only a few experiment-based examples have been documented [11–13]. Therefore, there is an urgent need of abundant experiment data about the relationship between structure and properties to advance the luminescence theory of uranyl ion in complexes.

As both coordination and hydrogen-bonding synthon, oxamate group has been proven to be versatile for the con-

*Corresponding author (email: liuws@lzu.edu.cn)

struction of functional transition-metal coordination polymers [14]. After the determination of the coordination mode between uranyl and oxalate through long-term efforts [15–19], it is necessary to inquire into the interaction between uranyl and oxamate by synthesizing and characterizing the resulting solid-state products, and further explore the potential for the sequestration of uranyl ions through selective crystallization.

In general, precipitation- or crystallization-based uranyl sequestration mainly refers to the sediment of uranyl ions with minerals [20,21]. More recently, we have proposed the selective crystallization of uranyl-organic complexes as a uranyl sequestration strategy [22,23], since crystallization is a convenient and environmental-friendly technique, and also the organic ligands are chemically tailored like those in solvent extraction strategy [24]. Although the crystallization experiments are carried out at a high uranium concentration level, the temperature range in the interior of hydrothermal reactor is similar to that in the interior of nuclear-waste storage tank [25,26]. In consideration of the water solubility, here we design *N*-substituted short-chain aliphatic bis(oxamate) ligands in their ethyl ester form, diethyl ethylene-1,2-dioxamate (DEEDO) and diethyl butylene-1,2-dioxamate (DEBDO) (Figure 1(a)), to react with uranyl ions in mild hydrothermal conditions.

2 Experimental

2.1 General experimental

All reagents were purchased commercially and used without further purification. The infrared spectrum was recorded on a Nicolet FT-170SX instrument (Nicolet, USA) using KBr discs in the 400–4000 cm^{-1} region. Powder X-ray diffraction (PXRD) patterns were collected with a PANalytical X'Pert Pro Diffractometer (PANalytical, Netherlands) operated at 40 kV and 40 mA with Cu-Kα radiation (step size: 0.02°; step time: 15 s). Elemental analyses were performed on an Elementar Analysenesysteme GmbH varioEL cube instrument (Elementar, Germany). Thermal analyses were conducted on a PYRIS Diamond TG/DTA instrument (PerkinElmer, USA). Fluorescence measurements were made on an FLS920 (Edinburgh Instruments, Britain). Luminescence decays were fitted by Eq. (1) on F900 software.

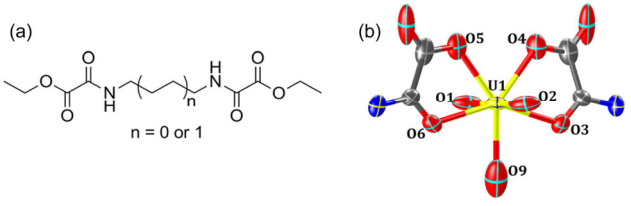

Figure 1 (a) The DEEDO and DEBDO precursors; (b) the uranium environment with ellipsoids is drawn at the 50% probability (color online).

The proportions of each lifetime components were calculated according to Eq. (2).

$$R(t) = B_1 e^{(-t/\tau_1)} + B_2 e^{(-t/\tau_2)} + \cdots + B_n e^{(-t/\tau_n)} \quad (1)$$

$$\tau_1\% = \frac{\tau_1 B_1}{\tau_1 B_1 + \tau_2 B_2 + \cdots + \tau_n B_n}$$
$$\tau_2\% = \frac{\tau_2 B_2}{\tau_1 B_1 + \tau_2 B_2 + \cdots + \tau_n B_n} \quad (2)$$
$$\cdots$$
$$\tau_n\% = \frac{\tau_n B_n}{\tau_1 B_1 + \tau_2 B_2 + \cdots + \tau_n B_n}$$

2.2 Synthesis of DEEDO and DEBDO

The DEEDO and DEBDO were synthesized according to the similar procedure of reference [27]. A solution of 1,2-ethylenediamine or 1,4-butylenediamine (20 mmol) and triethylamine (44 mmol) in dry CH_2Cl_2 (30 mL) was slowly added dropwise to a cooled (0 °C) solution of the ethyl oxalylchloride (44 mmol) in dry CH_2Cl_2 (50 mL). Stirring was continued for 30 min at 0 °C and overnight at room temperature. CH_2Cl_2 (50 mL) was added and the mixture washed with water, 1.5% AcOH, 5% $NaHCO_3$, and again with water. The organic layer was dried by Na_2SO_4 and the solvent evaporated to obtain white solid.

2.3 Synthesis of $[UO_2(EDO)(H_2O)]\cdot H_2O$ (compound 1)

A 20 mL vial was charged with $UO_2(NO_3)_2\cdot 6H_2O$ (18.8 mg, 0.0375 mmol), DEEDO (13 mg, 0.05 mmol), and distilled water (2 mL). The sample was heated at 75 °C for 12 h and then cooled to room temperature. The resulting yellow product was filtered off, washed with a little water, and dried at room temperature. Yield (based on UO_2^{2+}): 65%. IR (KBr, cm^{-1}): 3290 (vs), 3100 (m), 2348 (w), 1637 (vs), 1453 (s), 1352 (vs), 1269 (s), 1227 (s), 1047 (m), 933 (vs), 818 (s), 749 (s), 533 (s), 463 (s). Elemental analysis (%): calcd. for $C_6H_{10}N_2O_{10}U$ (508.19): C 14.17, H 1.97, and N 5.51; found: C 15.21, H 1.61, and N 5.53.

2.4 Synthesis of $[UO_2(BDO)(H_2O)]\cdot 2H_2O$ (compound 2)

A 20 mL vial was charged with $UO_2(NO_3)_2\cdot 6H_2O$ (18.8 mg, 0.0375 mmol), DEBDO (14.4 mg, 0.05 mmol), and distilled water (2 mL). The sample was heated at 75 °C for 12 h and then cooled to room temperature. A yellow polycrystalline solid was filtered off, washed with a little water, and dried at room temperature. Yield (based on UO_2^{2+}): 57%. IR (KBr, cm^{-1}): 3544 (m), 3328 (m), 3271 (m), 3084 (w), 2941 (w), 2348 (w), 1688 (vs), 1644 (vs), 1545 (m), 1456 (w), 1370 (s), 1345 (m), 1266 (m), 1196 (m), 1057 (w), 986 (w), 927 (s), 780 (m), 746 (m), 520 (m),

473 (m). Elemental analysis (%): calcd. for $C_8H_{16}N_2O_{11}U$ (554.3): C 17.64, H 2.94, and N 5.14; found: C 18.15, H 2.75, and N 5.08. The PXRD pattern of bulk sample as-synthesized is not very consistent with the simulated pattern (Figure S2, Supporting Information online). Cahill [28] has noticed an unknown secondary phase in the crystallization of uranyl long-chain aliphatic dicarboxylate coordination polymers. In this example, however, the uranyl oxamate unit should be always the same. The single crystal sample comes from the fragmented pieces.

2.5 Competition experiments

A 20 mL vial was charged with $UO_2(NO_3)_2\cdot 6H_2O$ (18.8 mg, 0.0375 mmol), one kind of competing metal nitrate (0.0375 mmol), DEEDO (13 mg, 0.05 mmol), and spring water (2 mL). The sample was heated at 75 °C for 12 h and then cooled to room temperature. The resulting yellow product was filtered off, washed with a little water, and dried at room temperature. Yield (based on UO_2^{2+}): >60%. Elemental analysis (%): C 15.26, H 1.63, and N 5.46.

2.6 Single-crystal structure determination

Single-crystal X-ray diffraction data were collected on a Bruker APEX-II CCD diffractometer (Germany) (Mo-Kα, $\lambda = 0.71073$ Å) at 293 K. An empirical absorption correction based on a comparison of redundant and equivalent reflections was applied using SADABS. Both structures were solved by direct methods and refined by fullmatrix least-squares cycles on F^2 (Table 1).

Table 1 Crystal data and structural refinement results

Compound	**1**	**2**
Formula	$[UO_2(EDO)(H_2O)]\cdot H_2O$	$[UO_2(BDO)(H_2O)]\cdot 2H_2O$
Formula weight	508.19	554.3
Temperature (K)	296(2)	296(2)
Crystal system	monoclinic	monoclinic
Space group	*P*2/*c*	*P*2/*n*
a (Å)	5.4930(14)	5.618(16)
b (Å)	7.0433(18)	8.34(2)
c (Å)	16.015(4)	15.46(4)
β (°)	99.081(2)	96.13(4)
V (Å^3)	611.8(3)	720(4)
Z	2	2
D_c (g cm^{-3})	2.759	2.529
Reflns coll.	4247	3326
Unique reflns	1086	746
R_{int}	0.0347	0.1249
R_1 [$I>2\sigma(I)$] [a]	0.0291	0.0574
wR_2 [$I>2\sigma(I)$] [b]	0.0564	0.1118
R_1 (all data)	0.0332	0.0718
wR_2 (all data)	0.0587	0.1201
GOF [b]	1.180	1.050

a) $R_1=\sum\{|F_o|-|F_c|\}/\sum|F_o|$; b) $wR_2=[\sum w(F_o^2-F_c^2)^2/\sum w(F_o^2)^2]^{1/2}$; b) Goodness of fit.

3 Results and discussion

3.1 Synthesis and structures

The bis(oxamate) ligands, ethylene-1,2-dioxamate (EDO^{2-}) and butylene-1,2-dioxamate (BDO^{2-}), are easily generated by hydrothermal reaction of DEEDO or DEBDO with uranyl ions at 75 °C; this process results in the formation of flat like rhombic crystals of $[UO_2(EDO)(H_2O)]\cdot H_2O$ (**1**) and $[UO_2(BDO)(H_2O)]\cdot 2H_2O$ (**2**). Single-crystal X-ray analyses reveal that compounds **1** and **2** are isostructural. Compounds **1** and **2** crystallize in the monoclinic space group *P*2/*c* and *P*2/*n* respectively. Their asymmetric units contain one mononuclear uranyl ion. The uranium coordination environment is shown in Figure 1(b). In addition to two oxo groups at the axial location (in **1**, U–O1 1.7228(1) Å; in **2**, U–O1 1.724(1) Å), the uranium atom is equatorially bound to four oxygen atom from two distinct ligands (in **1**, U–O at an average distance of 2.374 Å; in **2**, U–O at an average distance of 2.363 Å). Its last pentagonal bipyramidal coordination geometry is completed by one water molecule (in **1**, U–O9 2.3769(1) Å; in **2**, U–O9 2.492(3) Å).

As shown in Figure 2, compounds **1** and **2** consist of one-dimensional (1D) polymeric chain. Each bis(oxamate) ligand is coordinated to two uranium ions through the OO donor sets of its two oxamate groups, leaving potential hydrogen bonding donor (amide) and hydrogen bonding acceptor (carbonyl). As two bis(oxamate) ligands are in a cis arrangement around the uranium center, the polymeric chain adopts zigzag conformation. Owing to the presence of kinked aliphatic chain backbone, this type of 1D structure can be best described as stepwise zigzag chain. Furthermore, the adjacent chains are arranged in a parallel fashion and cross-linked by interchain hydrogen bonding interaction between amide N–H donor and carbonyl O acceptor, thus generating a 2D supramolecular layer with "step" conformation. Notably, the hydrogen bonding in **1** (H···O distance

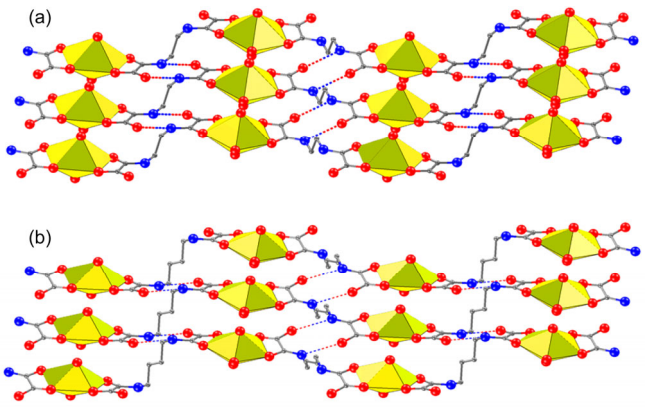

Figure 2 Polyhedral representation of 1D polymeric chain and 2D supramolecular layer of compound **1** (a) and compound **2** (b). Carbon- and nitrogen-bound hydrogen atoms are omitted (color online).

2.071 Å, N−H···O angle 144.14 Å, and N···O distance 2.814 Å) is much stronger than that in **2** (H···O distance 2.347 Å, N−H···O angle 133.86 Å, and N···O distance 3.007 Å). In **2**, the far separation between O and N is due to the flexible butylene spacer. Thermogravimetry (TG) analysis of **1** under a nitrogen atmosphere shows that the polymeric skeleton is stable up to ~300 °C and with no stable phase after the complete dehydration (Figure S4).

3.2 Photophysical properties of 1 and 2

As mentioned above, the uranyl photophysics is rather intricate. Especially for uranyl complexes, their emission band shifts and high luminescence decay exponents relative to free uranyl ions are confusing. The solid-state emission spectra of **1**, **2**, and $UO_2(NO_3)_2\cdot 6H_2O$ were recorded by excitation at 365 nm at room temperature (Figure 3). They all exhibit a characteristic band composed of six distinct peaks that reflects the vibronic structure of transition [29]. The vibrationally resolved emission spectrum has been applied in uranium detection assays such as detecting uranium in glasses, ceramics and living organisms [11]. The emission maxima of **1** and **2** are located at 515 and 514 nm, respectively bathochromic shift 6 and 5 nm compared to the emission maxima of $UO_2(NO_3)_2\cdot 6H_2O$ at 509 nm. The emission maxima of the uranyl monomer shift to lower energy, possibly because the strong oxamate OO donor in the equatorial plane makes the uranyl oxygen atoms more basic, thereby, leads to narrower HOMO-LUMO energy gap. The slightly larger shift of **1** than **2** may be owing to the increased strength of oxamate donor in **1**, whose N–H groups are stronger hydrogen-bonded. Here we may first demonstrate that the weak supramolecular interaction contributes to uranyl emission shift, further ensuring the ligand L feature of uranyl luminescence.

After excitation at 365 nm, the luminescence decay curves of both **1** and **2** are fitted well with triple-exponential function, showing lifetimes of 4.67±0.47 (2.98%), 24.32±0.29 (79.01%), and 45.06±1.26 (18.01%) μs for **1**, and 3.75±0.20 (8.84%), 16.35±0.29 (76.25%), and 30.54±1.41 (14.91%) μs for **2** (the percentage refers to the proportion of each component). But the emission of uranyl nitrate hexahydrate $[UO_2(NO_3)_2\cdot 6H_2O]$ excited at 365 nm exhibits a single-exponential decay with a lifetime of 739±1 μs. The luminescence intensities of both **1** and **2** are weaker than that of free uranyl ions, as the photophysical process is accompanied by the photochemical process [11,30,31]. Photoexcitation of UO_2^{2+} to higher excited states leads to the formation of UO_2^{2+}* with oxygen-centered radical. The UO_2^{2+}* can return to the ground state through luminescence, and can develop to the uranium(V) radical pair by taking an electron from organic group as well. As a consequence, the luminescence quantum yield is counter-related to the photochemical quantum yield. Moreover, the luminescence lifetimes of **1** are uniformly longer than those of **2** (Figure 4), showing that the stronger hydrogen bonding interaction is more likely to decrease the N–H vibration quenching, in good agreement with the actinide f feature of uranyl excited state. Given that the medium-long-lived components dominate the luminescence decays in both **1** and **2**, the longest-lived components may originate from the weak coupling of equatorial water vibration and axial O=U=O vibration that enhances absorption electronic transition [32], and the shortest-lived components may be due to the vibrational coupling of f-characterized excited state by N–H oscillators.

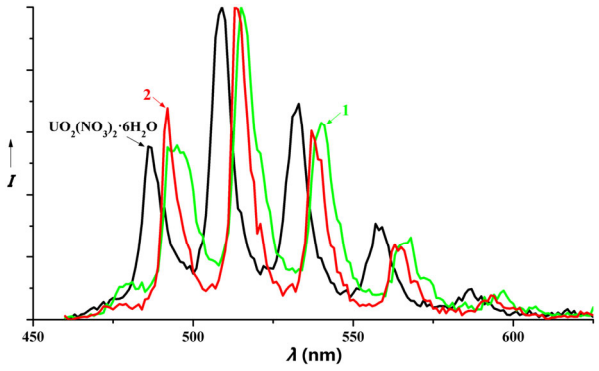

Figure 3 Solid-state emission spectra of $UO_2(NO_3)_2\cdot 6H_2O$, **1** and **2** at room temperature (color online).

3.3 Photophysics of uranyl oxalate trihydrate

To support these proposals on emission shift and multi-

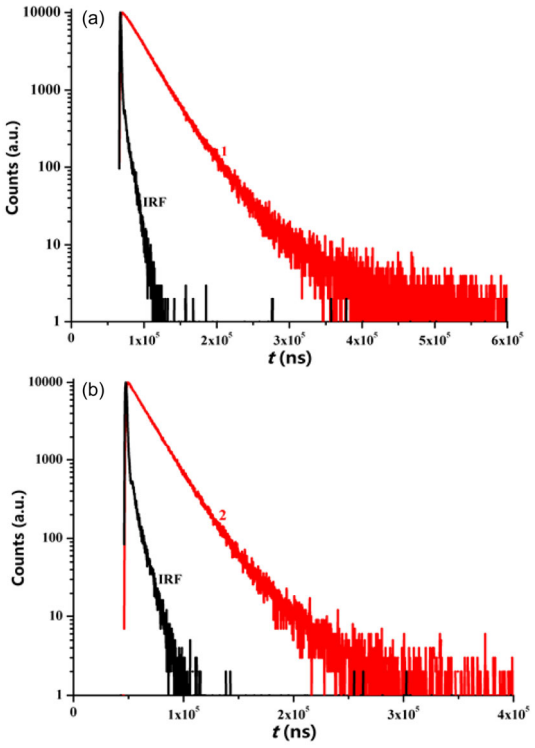

Figure 4 Luminescence decay profiles of **1** (a) and **2** (b) (color online).

exponential decay of uranyl ion in complexes, we reviewed the luminescence spectrum and decay curve of the uranyl-urea-bearing dipropionate compound featuring only N–H oscillators [22], and examined those of uranyl oxalate trihydrate [$UO_2C_2O_4\cdot 3H_2O$] possessing coordination environments and polymeric chain structure similar to **1** and **2** but no N–H oscillators (Figure 5) [15,16]. In comparison with $UO_2(NO_3)_2\cdot 6H_2O$, the uranyl-urea-bearing dipropionate compound shows no emission shift, but the luminescence decay curve fits double-exponential function. This may reveal the vibrational coupling of uranyl excited state with N–H oscillator. The lifetime values of uranyl-urea-bearing dipropionate and uranyl oxmate are at nearly the same order of magnitude, because the softer N atom contributes to photochemical process. The emission maxima of $UO_2C_2O_4\cdot 3H_2O$ shows only 1 nm bathochromic shift compared to that of $UO_2(NO_3)_2\cdot 6H_2O$ (Figure 6), because the bridging mode of oxalate makes its two sets of OO donors weaken. Excited at 365 nm, the emission of $UO_2C_2O_4\cdot 3H_2O$ exhibits double-exponential decay with lifetimes of 166±5 (22.05%) and 368±3 (77.95%) μs (Figure 7). This proves the remarkable effect of water on the promotion of the uranyl excited state. In a word, the luminescence intensity of uranyl ion in complexes is governed mainly by the photochemical process, while the N–H and water vibrational couplings cause multi-channel inactivation of uranyl excited state.

3.4 Uranyl sequestration

By view of the good crystallization capacity of **1**, we choose DEEDO to examine the performance of oxamate ligand in the sequestration of uranyl ions. With the addition of a comparable amount of competing metal cations (e.g., Na^+, K^+, Mg^{2+}, Ca^{2+}, Al^{3+}, Pb^{2+}, Mn^{2+}, Co^{2+}, Ni^{2+}, Cu^{2+}, Zn^{2+}, Cd^{2+}, Ce^{3+}, Tb^{3+}, or Yb^{3+}), reaction of DEEDO with uranyl ion in distilled water gives no crystalline product of **1**. While using alkaline spring water (pH around 7.3) as solvent, each kind of competing metal cation makes little effect on the crystallization and separation of uranyl species of **1**, confirmed by EA and PXRD of crystalline solid (see synthetic procedures and Figure 8). Besides the strongly geometrical preference for uranyl ion, the selectivity over other metal ions is more likely to be kinetic selectivity [33], as, in alkaline solution, the activation energy of the uranyl-synergized hydrolysis of DEEDO decreases much larger than those synergized by other metal ions, that is, the difference of Lewis acidity between uranium(VI) and other metal ions is magnified.

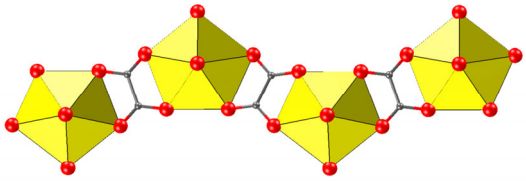

Figure 5 Polyhedral representation of 1D polymeric chain of $UO_2C_2O_4\cdot 3H_2O$ (color online).

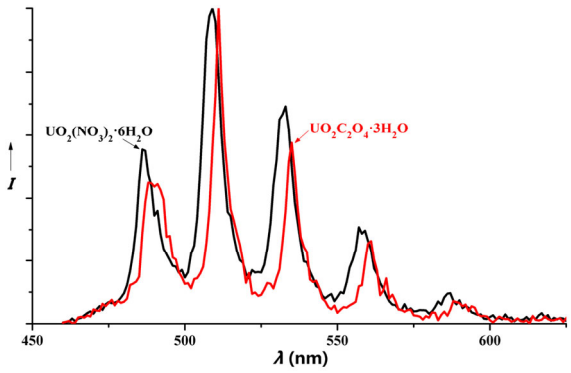

Figure 6 Solid-state emission spectra of $UO_2(NO_3)_2\cdot 6H_2O$ and $UO_2C_2O_4\cdot 3H_2O$ at room temperature.

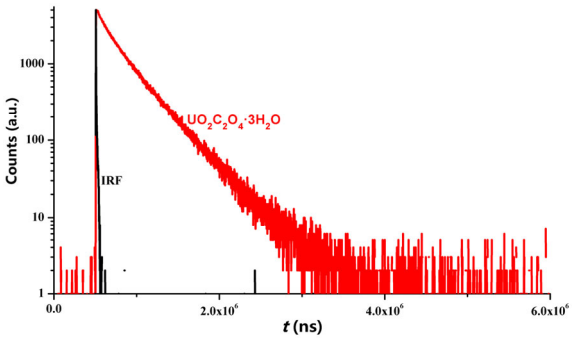

Figure 7 Luminescence decay profiles of $UO_2C_2O_4\cdot 3H_2O$ (color online).

4 Conclusions

In summary, we first exploited the oxamate ligands as uranyl complexing agents and succeeded in obtaining two isostructural crystalline compounds with identical stepwise

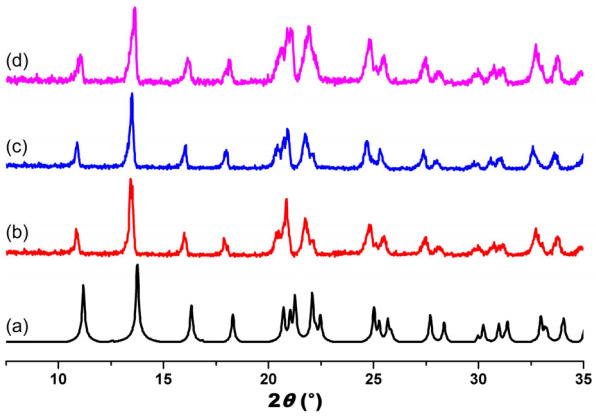

Figure 8 (a) Simulated powder XRD pattern of **1**, and the experimental powder XRD patterns of **1** (b) as-synthesized from distilled water, (c) as-synthesized from spring water, and (d) as-synthesized from spring water in the presence of competing metal cations.

zigzag chain structure and distinct interchain hydrogen bonding interaction. After rigorous experimental studies, we answered theoretical issues with regard to luminescence shift and multi-exponential decay, as well as application issue regarding the sequestration of uranyl ions through selective crystallization of uranyl complexes.

Acknowledgments This work was supported by the National Natural Science Foundation of China (21431002) and the Specialized Research Fund for the Doctoral Program of Higher Education (20110211130002).

Conflict of interest The authors declare that they have no conflict of interest.

Supporting information The supporting information is available online at http://chem.scichina.com and http://link.springer.com/journal/11426. The supporting materials are published as submitted, without typesetting or editing. The responsibility for scientific accuracy and content remains entirely with the authors.

1 Wang KX, Chen JS. *Acc Chem Res*, 2011, 44: 531–540
2 Andrews MB, Cahill CL. *Chem Rev*, 2013, 113: 1121–1136
3 Loiseau T, Mihalcea I, Henry N, Volkringer C. *Coord Chem Rev*, 2014, 266: 69–109
4 Yanga W, Parkerb TG, Sun ZM. *Coord Chem Rev*, 2015, 303: 86–109
5 Yudintsev SV, Stefanovsky SV, Ewing RC. Actinide host phases as radioactives waste forms. In: Krivovichev SV, Burns PC, Tananaev IG, Eds. *Structural Chemistry of Inorganic Actinide Compounds*. Amsterdam: Elsevier, 2007
6 Nash KL, Horwitz EP, Diamond H, Rickert PG, Muntean JV, Mendoza MD, Di Giuseppe G. *Solvent Extr Ion Exch*, 1996, 14: 13–33
7 Morss LR, Nash KL, Ensor DD. *J Chem Soc, Dalton Trans*, 2000: 285–291
8 Fourmigué M, Batail P. *Chem Rev*, 2004, 104: 5379–5418
9 Chernyshev AN, Morozov D, Mutanen J, Kukushkin VY, Groenhof G, Haukka M. *J Mater Chem C*, 2014, 2: 8285–8294
10 Denning RG. *J Phys Chem A*, 2007, 111: 4125–4143
11 Natrajan LS. *Coord Chem Rev*, 2012, 256: 1583–1603
12 Zheng YZ, Tong ML, Chen XM. *Eur J Inorg Chem*, 2005: 4109–4117
13 Borkowski LA, Cahill CL. *Cryst Growth Des*, 2006, 6: 2248–2259
14 Grancha T, Ferrando-Soria J, Castellano M, Julve M, Pasάn J, Armentano D, Pardo E. *Chem Commun*, 2014, 50: 7569–7585
15 Staritzky E, Cromer DT. *Anal Chem*, 1956, 28: 1353–1354
16 Jayadevan NC, Chackraburtty DM. *Acta Cryst Sec B*, 1972, 28: 3178–3182
17 Alcock NW. *J Chem Soc Dalton Trans*, 1973: 1610–1613
18 Jayadevan NC, Mudher KDS, Chackraburtty DM. *Acta Cryst Sec B*, 1975, 31: 2277–2280
19 Szabo Z, Fischer A. *Acta Cryst Sec E*, 2002, 58: i56–i58
20 Tokunaga TK, Kim Y, Wan J. *Environ Sci Technol*, 2009, 43: 5467–5471
21 Tokunaga TK, Kim Y, Wan J, Yang L. *Environ Sci Technol*, 2012, 46: 7471–7477
22 Shu YB, Xu C, Liu WS. *Eur J Inorg Chem*, 2013: 3592–3595
23 Shu YB, Ju ZH, Zhang HR, Liu WS. *Sci China Chem*, 2015, 58: 845–849
24 Riisiö A, Väisänen A, Sillanpää R. *Inorg Chem*, 2013, 52: 8591–8600
25 Rao L, Garnov AY, Jiang J, Di Bernardo P, Zanonato P, Bismondo A. *Inorg Chem*, 2003, 42: 3685–3692
26 Di Bernardo P, Zanonato P, Bismondo A, Jiang H, Garnov AY, Jiang J, Rao L. *Eur J Inorg Chem*, 2006, 4533–4540
27 Vujičić NŠ, Glasovac Z, Zweep N, van Esch JH, Vinković M, Popović J, Žinić M. *Chem Eur J*, 2013, 19: 8558–8572
28 Borkowski LA, Cahill CL. *Cryst Growth Des*, 2006, 6: 2241–2247
29 Brachmann A, Geipel G, Bernhard G, Nitsche H. *Radiochim Acta*, 2002, 90: 147–153
30 Li Y, Su J, Mitchell E, Zhang GQ, Li J. *Sci China Chem*, 2013, 56: 1671–1681
31 Tsushima S, Götz C, Fahmy K. *Chem Eur J*, 2010, 16: 8029–8033
32 Liu G, Deifel NP, Cahill CL, Zhurov VV, Pinkerton AA. *J Phys Chem A*, 2012, 116: 855–864
33 Zhang JP, Huang XC, Chen XM. *Chem Soc Rev*, 2009, 38: 2385–2396